Available online at www.sciencedirect.com
ScienceDirect
Trans. Nonferrous Met. Soc. China 24(2014) 2529−2535
Transactions of Nonferrous Metals Society of China
www.tnmsc.cn

Effects of surface nanocrystallization on corrosion resistance of β-type titanium alloy

Lei JIN[1], Wen-fang CUI[1], Xiu SONG[1], Gang LIU[2], Lian ZHOU[1,3]

1. Key Laboratory for Anisotropy and Texture of Materials (Ministry of Education), Northeastern University, Shenyang 110819, China;
2. Research Institute, Northeastern University, Shenyang 110819, China;
3. Northwest Institute for Nonferrous Metal Research, Xi'an 710016, China

Received 10 October 2013; accepted 10 February 2014

Abstract: Surface mechanical attrition treatment (SMAT) was performed on biomedical β-type TiNbZrFe alloy for 60 min at room temperature to study the effect of surface nanocrystallization on the corrosion resistance of TiNbZrFe alloy in physiological environment. The surface nanostructure was characterized by TEM, and the electrochemical behaviors of the samples with nanocrystalline layer and coarse grain were comparatively investigated in 0.9% NaCl and 0.2% NaF solutions, respectively. The results indicate that nanocrystallines with the size of 10−30 nm are formed within the surface layer of 30 μm in depth. The nanocrystallized surface behaves higher impedance, more positive corrosion potential and lower corrosion current density in 0.9% NaCl and 0.2% NaF solutions as compared with the coarse grain surface. The improvement of the corrosion resistance is attributed to the rapid formation of stable and dense passive film on the nanocrystallized surface of TiNbZrFe alloy.

Key words: biomedical β titanium alloy; surface nanocrystallization; electrochemical behavior; corrosion resistance

1 Introduction

β-type titanium alloys with non-toxic and allergen-free elements have been successfully developed for biomedical implants due to their low elastic modulus, high specific strength, excellent corrosion resistance and good biocompatibility [1−3]. However, there is still a problem that the surface of β-type titanium alloy is encapsulated by fibrous tissue without producing any osseous junctions with surrounding tissues after implantation. Moreover, the surface structures of the implants in body are very sensitive to fatigue fracture, wear and corrosion. Thus, the surface modification on the biomaterials becomes hot research topic and attracts more and more attentions.

Recently, the surface self-nanocrystallization on metal materials has been newly developed. It has been reported that nano-functionalized surface has promising properties in clinical application, such as high strength and hardness, excellent tribological properties as well as good bioactivity as compared with the course grain materials [4−6]. In addition, it can be easily achieved by means of various surface techniques, such as surface mechanical attrition treatment (SMAT) [7], high energy shot peening (HESP) [8], ultrasonic shot peening (USP) [9], laser shock peening (LSP) [10] and high velocity oxygen-fuel flame (HVOF) [11]. Among them, SMAT is an effective way to refine the grains into nanometer scale, which is achieved by heavy cold deformation without changing chemical compositions [12].

Up to date, the surface self-nanocrystallization has already been successfully performed on some metals and alloys, such as Fe, 304 stainless steel, Al alloy, Cu, Mg alloy and commercial pure Ti [13−17]. The effects of nanocrystallization on the corrosion resistance of alloys have different results. One of the viewpoints thought that the nanocrystallization usually leads to the decrease of corrosion properties due to the high chemical activity at grain boundaries [18]. But the other results indicated that the effect of nanocrystallization on corrosion resistance depends on the alloy systems [18−23]. MISHRA [22]

Foundation item: Projects (N100702001, N120310001) supported by the Fundamental Research Funds for the Central Universities, China; Project (20131036) supported by Doctoral Fund of Liaoning Province, China; Project (51301037) supported by the National Natural Science Foundation of China

Corresponding author: Wen-fang CUI; Tel: +86-24-83691581; Fax: +86-24-23906316; E-mail: cuiwf@atm.neu.edu.cn

DOI: 10.1016/S1003-6326(14)63379-3

demonstrated that nanocrystalline Ni made by electro-deposition offered the superior resistance to localized corrosion. The nanocrystalline surface of 304 stainless steel produced by sandblasting and annealing treatment also showed the better corrosion properties [23]. Up to date, the corrosion mechanisms of nanocrystalline have not been well understood yet.

In the present investigation, a new biomedical β-type TiNbZrFe alloy was treated by SMAT. The surface nano-structure was characterized by TEM. The electrochemical behaviors of the surface nanocrystalline layer in 0.9% NaCl and 0.2% NaF solution were studied, respectively. The corrosion mechanism of surface nanocrystallinzation was analyzed. The effect of self-nanocrystallization prepared by SMAT on the corrosion behavior in physiological environment was discussed.

2 Experimental

The nominal composition of the tested material is 30% Nb, 8.8% Zr, 0.8% Fe, balance of Ti (mass fraction). The ingot was remelted in cold crucibles by vacuum electromagnetic suspension for three times, followed by hot forging to square billet at 850−900 °C. The samples with the size of 100 mm×50 mm×3 mm were cut from the square billet, and then solution treated at 850 °C for 0.5 h followed by water quenching. The surface of the samples were ground using SiC papers of 200−1200 meshes, and then ultrasonically cleaned with acetone, ethanol and distilled water. The SMAT test was performed using stainless steel balls in diameter of 8 mm in vacuum at room temperature. The sample was fixed on the upper part of the container. The bottom of the container was connected to a vibration device with frequency of 50 Hz. The testing duration was 60 min. After SMAT, the sample surface was slightly electropolished in 5% HCl + C_2H_5OH solution at room temperature to remove the impurities and eliminate the effects of roughness on the corrosion performance. The deformed microstructure on the surface layer was examined using TECNAI G^2 transmission electron microscope (TEM) with an acceleration voltage of 200 kV.

Electrochemical experiments were carried out by electrochemical workstation using three-electrode cell in 0.9% NaCl and 0.2% NaF solutions, which simulate the physiological and oral environment, respectively [24]. The electrochemical behaviors of the surface nanocrystalline and coarse grain samples were comparatively investigated. The electrochemical impedance spectroscopy (EIS) was measured by applying the sinusoidal potential perturbation of 5 mV at the open circuit potentials with frequency from 10 kHz to 10 MHz in logarithmic increment. Potentiodynamic polarization (PDP) behaviors were evaluated in the potential range from −1 V to 1 V and the scanning rate of 1 mV/s. Open circuit potentials (OCP) were continuously measured in 0.9% NaCl and 0.2% NaF solutions within 120 h. Before the electrochemical testing, the samples were immersed in the solution for about 30 min until the primarily corrosion potential reached a steady state. The surface morphologies of the corroded samples were observed by JEOL scanning electron microscope (SEM).

3 Results and discussion

3.1 Surface nanostructure

The surface morphologies of the SMAT sample are shown in Fig. 1. Some iron powders exfoliated from stainless steel balls are retained on the surface of the sample (Fig. 1(a)). After slightly electrochemical polishing, the iron powders are completely eliminated. At the same time, the surface roughness of the sample decreases obviously and no crack is seen on the surface of the sample (Fig. 1(b)). TEM images and the corresponding selected area electron diffraction (SAED) pattern of the deformed layer near the surface are shown in Fig. 2. It can be seen that the nanocrystallines with random orientation and distribution are formed. The nanocrystalline size ranges from 10 nm to 30 nm. By observation of the deformed microstructure at different

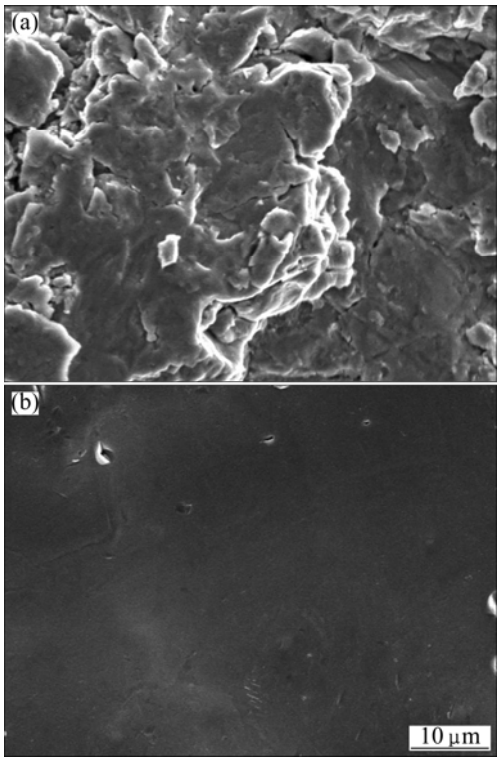

Fig. 1 Surface morphologies of SMAT sample before (a) and after (b) electropolishing treatment

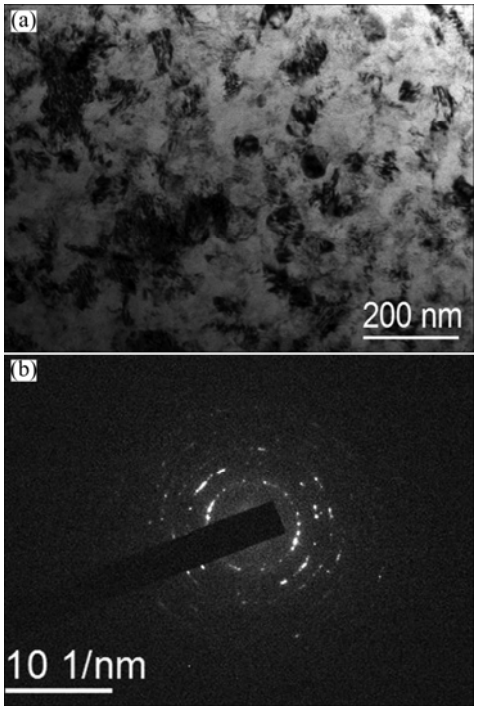

Fig. 2 TEM images of surface nanocrystallines of SMAT sample: (a) Bright field; (b) SAED pattern

layers, it was found that the depth of nanocrystalline layer is about 30 μm. The formation of nanocrystalline in TiNbZrFe alloy can be attributed to the high energy and high speed impact of a large number of stainless steel balls, which results in severe plastic deformation near the surface of the sample. During SMAT process, the rapid increase of dislocation density due to multisystem slip causes high strain energy within primary grains that drives the localized lattice rotation, forming a large number of micro- or nanocrystallines with large angle grain boundaries. Figure 3 shows the HRTEM image of the nanocrystalline in the surface deformed layer, showing the nanocrystallines with different crystal orientations and perfect lattice within the nanocrystallines.

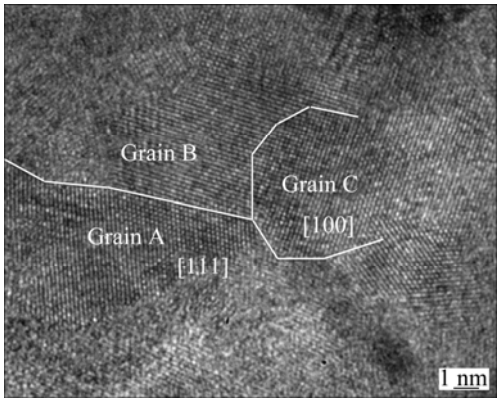

Fig. 3 HRTEM image of nanocrystallines of SMAT sample near surface layer

3.2 Electrochemical properties

The impedance spectra of SMAT and non-SMAT samples in 0.9% NaCl and 0.2% NaF solutions are shown as Bode and Nyquist plots in Fig. 4. It is known that the impedance at low frequency of Bode plots represents the corrosion resistance of the samples [25]. High impedance value reflects good corrosion resistance and low corrosion rate. It is seen from Figs. 4(a) and (b) that the impedance of surface nanocrystallized sample in 0.9% NaCl and 0.2% NaF solution are higher than that of the coarse grain sample. The feature is more obvious in 0.9% NaCl solution, indicating the better corrosion resistance of surface nanocrystallized sample in chloride ions containing environment.

Only one time constant in Bode plots ($-\theta$ versus lg f in Figs. 4(c) and (d)) shows a single layer structure on the sample surface. The phase angle at low frequency range of SMAT sample is higher than that of non-SMAT sample and remains close to 90° over a wide range of frequency, which indicates that the typical thin passive film with high impedance and low capacity is preferentially formed on the nanocrystalline surface. The dense passive film protects the metal matrix from the erosion of corrosive solution, inhibits corrosion reaction and decreases corrosion rate. The curvature radius of the curve in Nyquist plot presents electron transit process. The larger curvature radius of SMAT sample in Figs. 4(e) and (f) shows stronger inhibition effect for electron transiting and improved corrosion resistance due to surface nanocrystallization.

The equivalent circuit fitted with the EIS data is shown as $R_s(Q_pR_p)$ model, as shown in Fig. 5. Where R_s is the solution resistance, R_p is the passive film resistance and Q_p is the constant-phase element for the passive film. The electrochemical parameters of the equivalent circuit are shown in Table 1. In this model, the passive film is considered to be a parallel circuit of a resistor due to the ionic conduction through the film and capacitor due to its dielectric properties. This system describes an ideal capacitor for n=1, an ideal resistor for n=0 and n=−1 for a pure inductor. Table 1 shows that the values of n at different conditions are close to 1. Thus, both SMAT and non-SMAT samples can be described as an ideal capacitor. But R_p value of SMAT sample is one order of magnitude higher than that of non-SMAT sample, which indicates the denser and thicker passive film formed on SMAT sample in comparison with the non-SMAT sample.

Potentiodynamic polarization curves of both the samples in 0.9% NaCl and 0.2% NaF solutions are shown in Fig. 6. The corrosion potential φ_{corr} and the corrosion current density J_{corr} measured from the polarization curves are listed in Table 2. It can be seen that SMAT sample has higher corrosion potential and

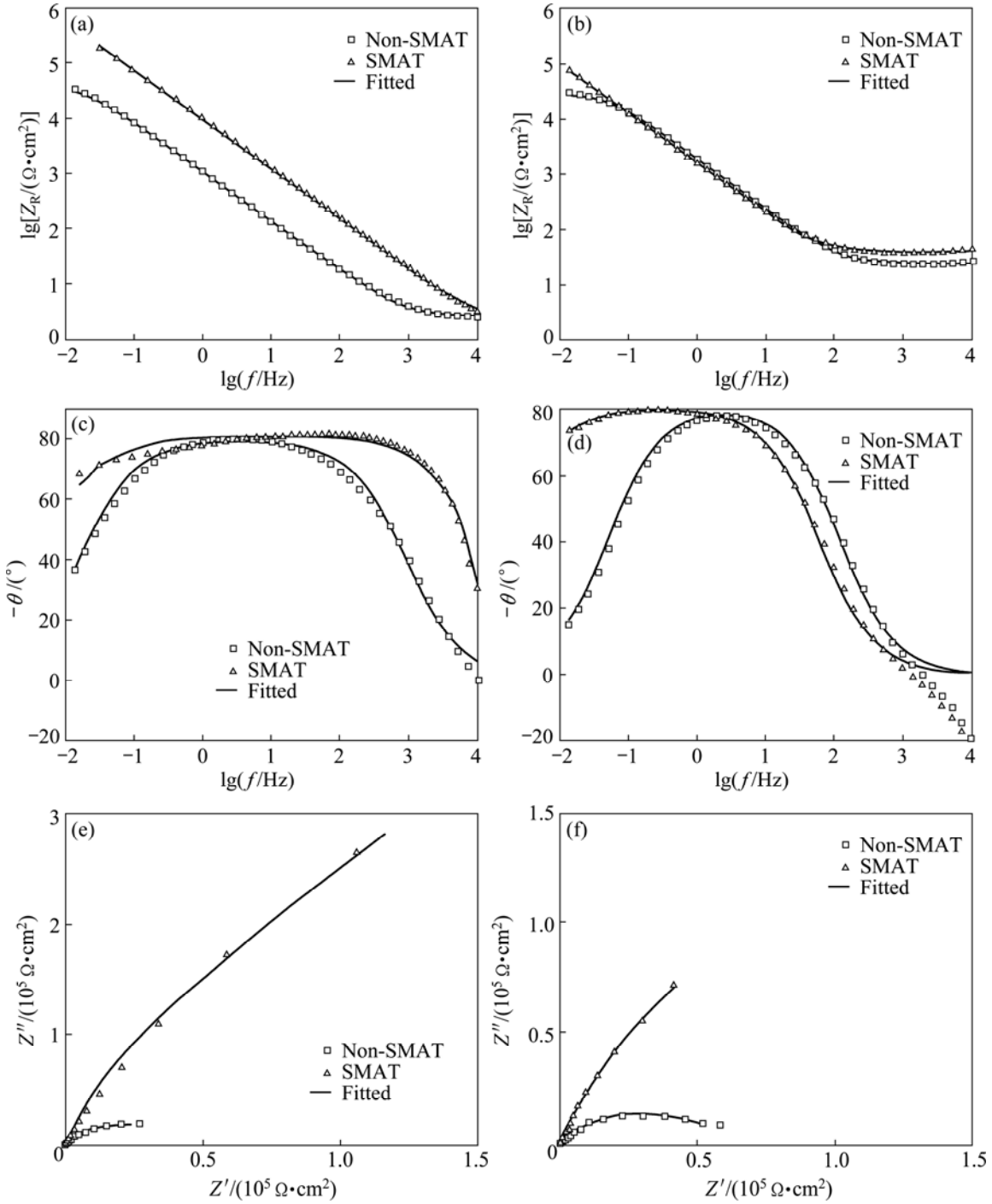

Fig. 4 Bode and Nyquist plots of SMAT and non-SMAT samples in 0.9% NaCl (a, c, e) and 0.2% NaF (b, d, f) solutions: (a, b) lg|Z_R| versus lg f; (c,d) $-\theta$ versus lg f; (e, f) Nyquist plots

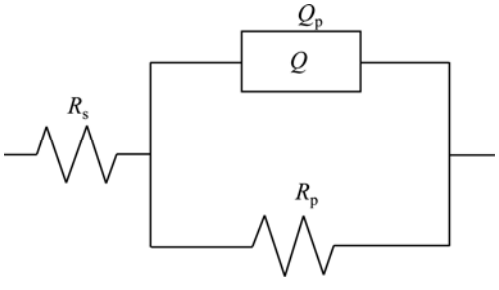

Fig. 5 Equivalent circuit model for EIS analysis

Table 1 Fitted EIS parameters of SMAT and non-SMAT samples in 0.9% NaCl and 0.2% NaF solutions

Sample	Solution	R_s/ (Ω·cm²)	Q_p/ ($\Omega^{-1}s^n$·cm^{-2})	n_p	R_p/ (Ω·cm²)
Non-SMAT	0.9%	2.59	1.790×10^{-4}	0.89	4.43×10^{4}
SMAT	NaCl	2.34	1.995×10^{-5}	0.90	9.42×10^{5}
Non-SMAT	0.2%	24.65	9.784×10^{-5}	0.91	2.96×10^{4}
SMAT	NaF	40.41	1.189×10^{-4}	0.90	5.65×10^{5}

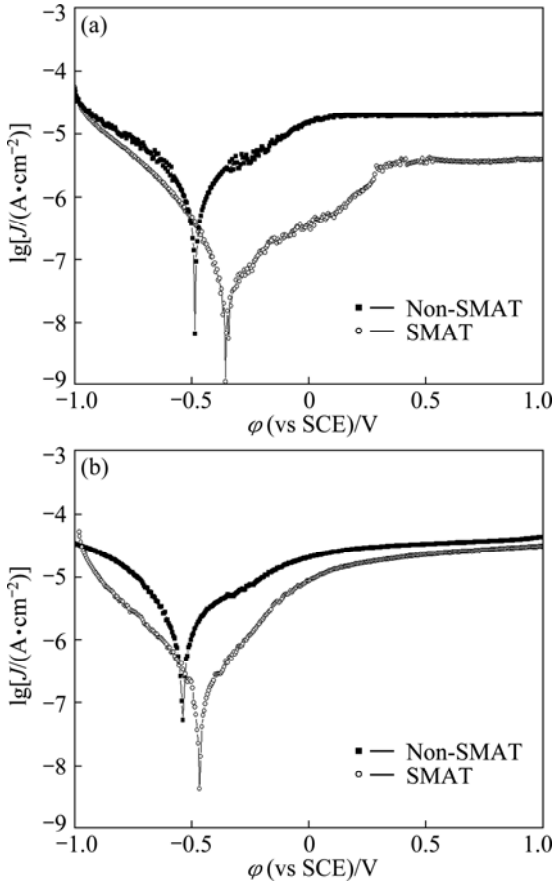

Fig. 6 Potentiodynamic polarization curves of SMAT and non-SMAT samples in 0.9% NaCl (a) and 0.2% NaF (b) solutions

Table 2 Electrochemical parameters obtained from potentiodynamic polarization curves

Sample	Solution	φ_{corr}/ V	J_{corr}/ (A·cm^{-2})	b_a/ mV	b_c/ mV
Non-SMAT	0.9%	−0.486	1.48×10^{-7}	18.34	−22.28
SMAT	NaCl	−0.355	1.70×10^{-8}	7.91	−19.74
Non-SMAT	0.2%	−0.537	2.20×10^{-7}	19.81	−20.39
SMAT	NaF	−0.467	2.59×10^{-8}	20.41	−28.57

lower corrosion current density than the non-SMAT sample, even if in 0.2% NaF solution. The anodic polarization curves of both samples in 0.9% NaCl and 0.2% NaF solutions display passivation feature, indicating the passive film formed on SMAT or non-SMAT sample. Nevertheless, the protective effect of the passive film on SMAT sample seems to be stronger than that on non-SMAT samples according to the results based on EIS and electrochemical parameters.

The eroded surface morphologies of SMAT and non-SMAT samples in 0.2% NaF solution were observed by SEM, as shown in Fig. 7. The corrosion pits with diameter below 300 nm densely distribute on the surface of non-SMAT sample, while the surface of SMAT sample is smooth and covered with dense oxide film. The surface morphologies of the two samples corroded in 0.9% NaCl solution show the similar results in spite of only slight corrosion for the non-SMAT sample. The observation of corroded surface proves again that surface nanocrystallization by SMAT can obviously enhance the corrosion resistance of β-type TiNbZrFe alloy in Cl^- and F^- ions containing environment.

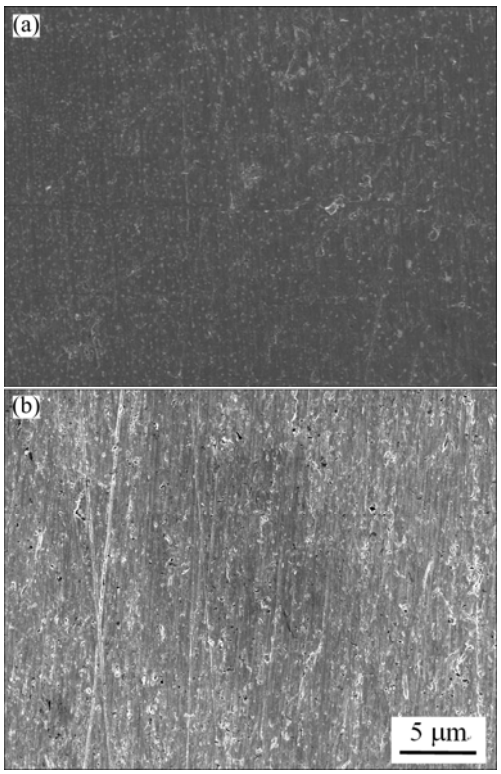

Fig. 7 SEM images of eroded surfaces of SMAT (a) and non-SMAT (b) samples in 0.2% NaF solution

Figure 8 shows the change of OCP of SMAT and non-SMAT samples as a function of immersion time in 0.9% NaCl and 0.2% NaF solutions. The initial potential of the SMAT sample in 0.9% NaCl solution is about −160 mV. After slight decreasing, OCP begins to rise slowly and attains stable state at the value of −150 mV. While OCP value of non-SMAT sample increases with immersion time, but always keeps more negative value as compared with SMAT sample. In 0.2% NaF solution, the OCP of non-SMAT sample rapidly increases at initial immersion and then keeps stable value of −260 mV. Nevertheless, the OCP of the SMAT sample behaves constant value of −170 mV, which is more positive than that of non-SMAT sample.

The value of OCP mainly indicates the tendency of corrosion reaction on electrode surface. The more positive OCP value of SMAT sample can be attributed to the rapid formation of ceramic film on nanostructure

surface, which makes the alloy be of better chemical stability through decreasing the diffusion of corrosive ions and the activity of charge carriers at the interface between solution and alloy. It is believed that the surface nanocrystalline supplies high density of nucleation sites for passive film, which is helpful to the formation of dense passive layer and the reduction of corrosion rate.

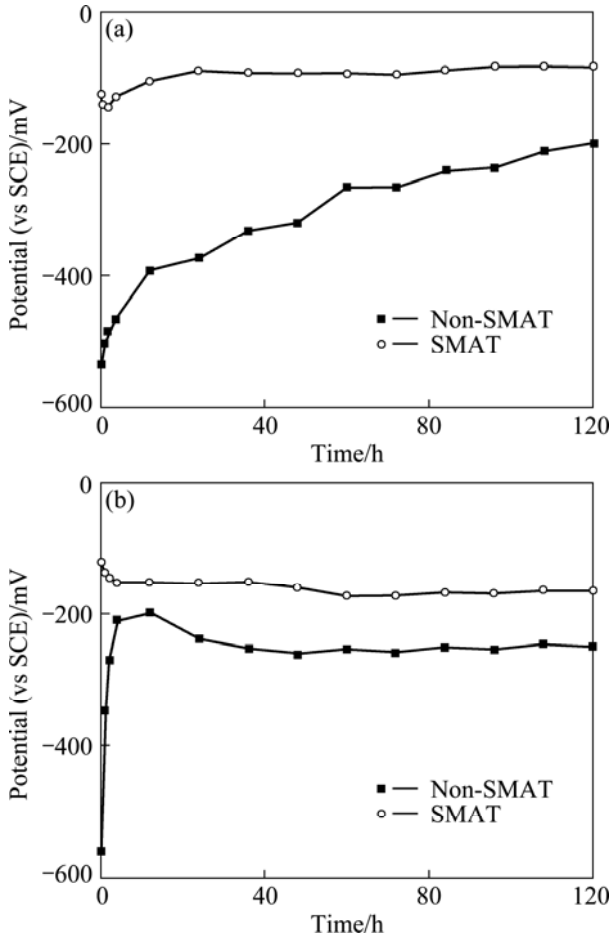

Fig. 8 OCP of SMAT and non-SMAT samples as a function of immersion time in 0.9% NaCl (a) and 0.2% NaF (b) solutions

4 Conclusions

1) Nanostructure surface layer is successfully prepared on β-type TiNbZrFe alloy by SMAT for 60 min. The equiaxed nanocrystallines with size of 10 to 30 nm are formed within the layer of 30 μm in depth from the surface.

2) SMAT sample behaves higher impedance, more positive corrosion potential and lower corrosion current density as compared with the non-SMAT sample in 0.9% NaCl and 0.2% NaF solutions. These are attributed to the preferential formation of the dense passive film on the nanocrystalline surface, which effectively improves the corrosion resistance of TiNbZrFe alloy in physiological environment.

References

[1] WANG K. The use of titanium for medical applications in the USA [J]. Materials Science and Engineering A, 1996, 213(1−2): 134−137.

[2] KURODA D, NIINOMI M, MORINAGA M, KATO Y, YASHIRO T. Design and mechanical properties of new β type titanium alloys for implant materials [J]. Materials Science and Engineering A, 1998, 243(1−2): 244−249.

[3] ZHANG D C, MAO Y F, YAN M, LI J J, SU E L, LI Y L, TAN S W, LIN J G. Superelastic behavior of a β-type titanium alloy [J]. Journal of the Mechanical Behavior of Biomedical Materials, 2013, 20: 29−35.

[4] WEBSTER T J, EJIOFOR J U. Increased osteoblast adhesion on nanophase metals: Ti, Ti6Al4V, and CoCrMo [J]. Biomaterials, 2004, 25(19): 4731−4739.

[5] ANTUNES R A, OLIVERIRA M C L. Corrosion fatigue of biomedical metallic alloys: Mechanisms and mitigation [J]. Acta Biomaterialia, 2012, 8(3): 937−962.

[6] MA Guo-zheng, XU Bin-shi, WANG Hai-dou, SI Hong-juan, YANG Da-xiang. Effect of surface nanocrystallization on the tribological properties of 1Cr18Ni9Ti stainless steel [J]. Materials Letters, 2011, 65(9): 1268−1271.

[7] SAMIH Y, BEAUSIR B, BOLLE B, GROSDIDIER T. In-depth quantitative analysis of the microstructures produced by surface mechanical attrition treatment (SMAT) [J]. Materials Characterization, 2013, 83: 129−138.

[8] LIU Gang, WANG Su-cheng, LOU Xin-fang, LU Jian, LU Ke. Low carbon steel with nanostructured surface layer induced by high-energy shot peening [J]. Scripta Materialia, 2001, 44(8−9): 1791−1795.

[9] LIU Gang, LU Jian, LU Ke. Surface nanocrystallization of 316L stainless steel induced by ultrasonic shot peening [J]. Materials Science and Engineering A, 2000, 286(1): 91−95.

[10] YE Chang, SUSLOV S, FEI Xue-ling, CHENG G J. Bimodal nanocrystallization of NiTi shape memory alloy by laser shock peening and post-deformation annealing [J]. Acta Materialia, 2011, 59(19): 7219−7227.

[11] XU Kai-dong, WANG Ai-hua, WANG Yang, DONG Xuan-pu, ZHANG Xiang-lin, HUANG Zao-wen. Research on a new technology of surface nanocrystallization in Mg alloy induced by HVOF microparticles impact [J]. Rare Metal Materails and Engineering, 2011, 40(7): 1271−1276. (in Chinese)

[12] LU Ke, LU Jian. Nanostructured surface layer on metallic materials induced by surface mechanical attrition treatment [J]. Materials Science and Engineering A, 2004, 375−377: 38−45.

[13] ARIFVIANTO B, SUYITNO, MAHARDIKA M. Effects of surface mechanical attrition treatment (SMAT) on a rough surface of AISI 316L stainless steel [J]. Applied Surface Science, 2012, 258(10): 4538−4543.

[14] BLONDE R, CHAN H L, BONASSO N A, BOLLE B, GROSDIDIERA T, LU J. Evolution of texture and microstructure in pulsed electro-deposited cu treated by surface mechanical attrition treatment (SMAT) [J]. Journal of Alloys and Compounds, 2010, 504(S1): s410−s413.

[15] MAO Xiang-yang, LI Dong-yang, WANG Zhang-zhong, ZHAO Xiu-ming, CAI Lu. Surface nanocrystallization by mechanical punching process for improving microstructure and properties of Cu−30Ni alloy [J]. Transactions of Nonferrous Metals Society of China, 2013, 23(6): 1694−1700.

[16] CHANG H W, KELLY P M, SHI Y N, ZHANG M X. Effect of eutectic Si on surface nanocrystallization of Al−Si alloys by surface

mechanical attrition treatment [J]. Materials Science and Engineering A, 2011, 530: 304−314.

[17] ZHU K Y, VASSEL A, BRISSET F, LU K, LU J. Nanostructure formation mechanism of α-titanium using SMAT [J]. Acta Materialia, 2004, 52(14): 4101−4110.

[18] GARBACZ H, PISAREK M, KURZYDLOWSKI K J. Corrosion resistance of nanostructured titanium [J]. Biomolecular Engineering, 2007, 24(5): 559−563.

[19] BALUSAMY T, SANKARA NARAYANAN T S N, RAVICHANDRAN K, PARK S, LEE M H. Influence of surface mechanical attrition treatment (SMAT) on the corrosion behaviour of AISI 304 stainless steel [J]. Corrosion Science, 2013, 74: 332−344.

[20] MARECI D, CHELARIU R, BOLAT G, CAILEAN A, GRANCEA V, SUTIMAN D. Electrochemical behaviour of Ti alloys containing Mo and Ta as β-stabilizer elements for dental application [J]. Transactions of Nonferrous Metals Society of China, 2013, 23(12): 3829−3836.

[21] LI Nan, LI Ying, WANG Sheng-gang, WANG Fu-hui. Electrochemical corrosion behavior of nanocrystallized bulk 304 stainless steel [J]. Electrochimica Acta, 2006, 52(3): 760−765.

[22] MISHRA R, BALASUBRAMANIAM R. Effect of nanocrystalline grain size on the electrochemical and corrosion behavior of nickel [J]. Corrosion Science, 2004, 46(12): 3019−3029.

[23] WANG X Y, LI D Y. Mechanical and electrochemical behavior of nanocrystalline surface of 304 stainless steel [J]. Electrochimica Acta, 2002, 47(24): 3939−3947.

[24] KANEKO K, YOKOYAMA K, MORIYAMA K, ASAOKA K, SAKAI J, NAGUMO M. Delayed fracture of beta titanium orthodontic wire in fluoride aqueous solutions [J]. Biomaterials, 2003, 24: 2113−2120.

[25] PALOMINO L M, SUEGAMA P H, AOKI I V, MONTEMOR M F, MELO H G D. Electrochemical study of modified non-functional bis-silane layers on Al alloy 2024-T3 [J]. Corrosion Science, 2008, 50(5): 1258−1266.

表面纳米化对β型钛合金耐腐蚀性能的影响

金 磊[1]，崔文芳[1]，宋 秀[1]，刘 刚[2]，周 廉[1,3]

1. 东北大学 材料织构与各向异性教育部重点实验室，沈阳 110819；
2. 东北大学 研究院，沈阳 110819；
3. 西北有色金属研究院，西安 710016

摘 要：采用表面机械研磨处理(SMAT)方法对医用 β 型 TiNbZrFe 合金表面处理 60 min，研究表面纳米化对 TiNbZrFe 合金在生理环境下耐腐蚀性能的影响。采用 TEM 观察表层纳米晶微观结构特征，采用电化学方法研究表面为粗晶与纳米晶的 TiNbZrFe 合金在 0.9% NaCl 和 0.2% NaF 溶液环境下的电化学行为。结果表明：TiNbZrFe 合金表面形成深度约 30 μm 的纳米晶层，纳米晶尺寸为 10~30 nm。在 0.9% NaCl 和 0.2% NaF 腐蚀环境下，与粗晶表面相比，表面为纳米晶的合金表现出较高的电阻、较正的自腐蚀电位以及较低的自腐蚀电流密度。合金耐腐蚀性能的提高主要归因于在纳米化的 TiNbZrFe 合金表面能够快速形成致密且稳定的钝化膜。

关键词：医用β型钛合金；表面纳米化；电化学行为；耐腐蚀性能

(Edited by Chao WANG)